Kinetic Models for Space Plasmas: Recent Progress for the Solar Wind and the Earth's Magnetosphere

V. Pierrard[1,2, a)], S. P. Moschou[1,3], M. Lazar[3,4], K. Borremans[1], and G. Lopez Rosson[1]

[1] *Royal Belgian Institute for Space Aeronomy (BIRA-IASB), Space physics and Solar-Terrestrial Center of Excellence (STCE), 3 av. Circulaire, B-1180 Brussels, Belgium*
[2] *Université Catholique de Louvain (UCL), Center for Space Radiations (CSR) and Georges Lemaître Centre for Earth and Climate Research (TECLIM), Earth and Life Institute (ELI), Place Louis Pasteur 3 bte L4.03.08, B-1348 Louvain-La-Neuve, Belgium*
[3] *Centre for mathematical Plasma Astrophysics, Department of Mathematics, KU Leuven, Celestijnenlaan 200B, 3001 Heverlee, Belgium*
[4] *Theoretical Physics IV, Ruhr University Bochum, D-44780 Bochum, Germany*

[a)]Corresponding author: viviane.pierrard@aeronomie.be

Abstract. Recent models for the solar wind and the inner magnetosphere have been developed using the kinetic approach. The solution of the evolution equation is used to determine the velocity distribution function of the particles and their moments. The solutions depend on the approximations and assumptions made in the development of the models. Effects of suprathermal particles often observed in space plasmas are taken into account to show their influence on the characteristics of the plasma, with specific applications for coronal heating and solar wind acceleration. We describe in particular the results obtained with the collisionless exospheric approximation based on the Lorentzian velocity distribution function for the electrons and its recent progress in three dimensions.
The effects of Coulomb collisions obtained by using a Fokker-Planck term in the evolution equation were also investigated, as well as effects of the whistler wave turbulence at electron scale and the kinetic Alfven waves at the proton scale. For solar wind especially, modelling efforts with both magnetohydrodynamic and kinetic treatments have been compared and combined in order to improve the predictions in the vicinity of the Earth. Photospheric magnetograms serve as observational input in semi-empirical coronal models used for estimating the plasma characteristics up to coronal heliocentric distances taken as boundary conditions in solar wind models.
The solar wind fluctuations may influence the dynamics of the space environment of the Earth and generate geomagnetic storms. In the magnetosphere of the Earth, the trajectories of the particles are simulated to study the plasmasphere, the extension of the ionosphere along closed magnetic field lines and to better understand the physical mechanisms involved in the radiation belts dynamics.

INTRODUCTION : NON-THERMAL VELOCITY DISTRIBUTION FUNCTIONS

Kinetic models have been developed to give a microscopic description of space plasmas that is extremely useful in such rarefied environments. Indeed, the velocity distribution functions $f(\mathbf{r},\mathbf{v},t)$ of the particles (where $\mathbf{r}$, $\mathbf{v}$ and t are, respectively, the position and the velocity of the particles, and the time) are generally non-Maxwellian and anisotropic in low density plasmas where the collisions are rare. The distributions are often observed to decrease as a power law of the square velocity instead of exponentially and thus to have more suprathermal particles in their tails. This is illustrated in Fig. 1 for the electrons observed in situ in the solar wind, here at 2.7 AU by ULYSSES. This excess of suprathermal particles is

30th International Symposium on Rarefied Gas Dynamics
AIP Conf. Proc. 1786, 160001-1–160001-10; doi: 10.1063/1.4967658
Published by AIP Publishing. 978-0-7354-1448-8/$30.00

also observed at other radial distances and for other particles species (ions and protons), not only in the solar wind but also in the magnetosphere of the Earth and other planets (see [1] for a review).

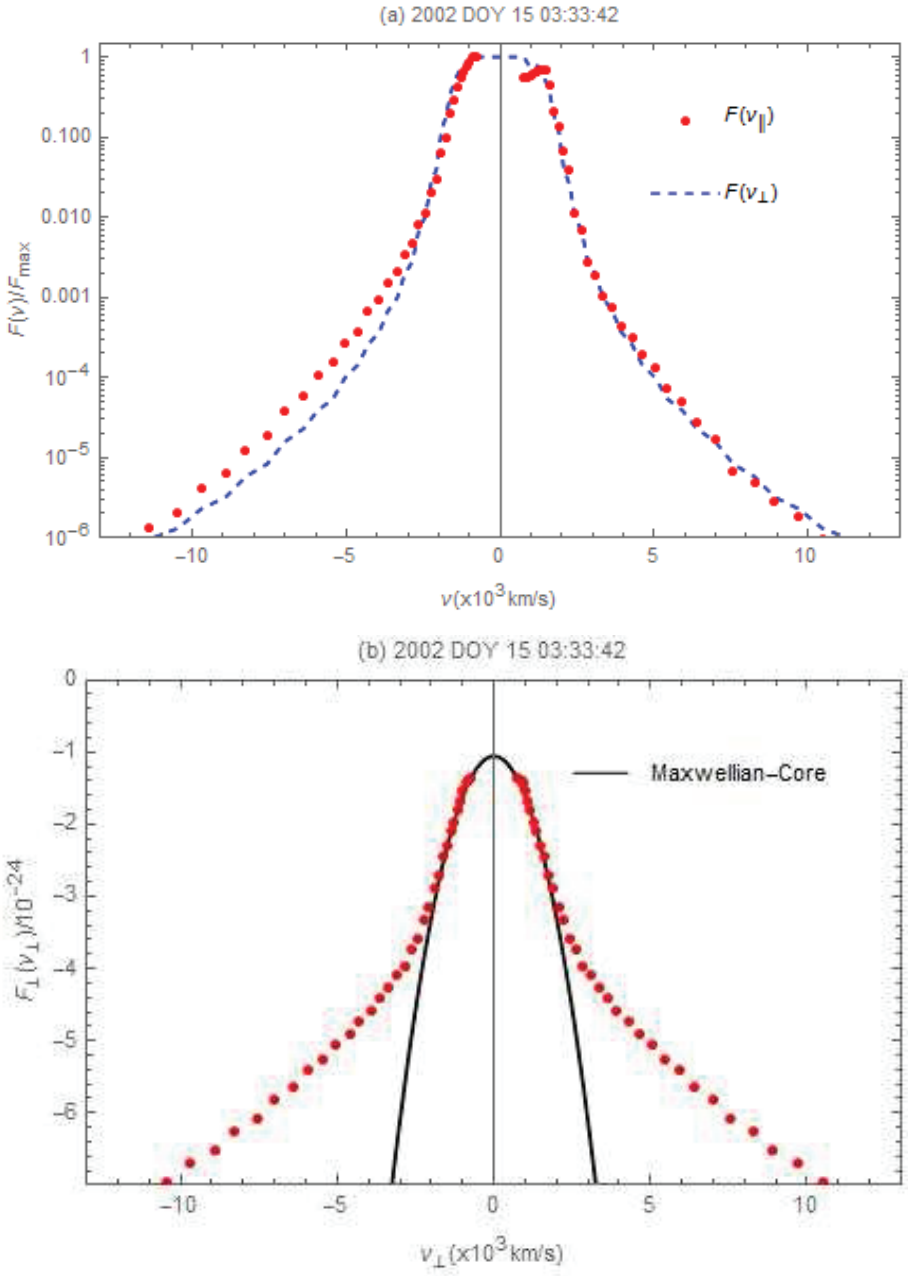

FIGURE 1. Upper panel: Non-Maxwellian electron velocity distribution observed in-situ in the solar wind at 2.7 AU by ULYSSES in the direction parallel (red dots) and perpendicular (blue-dashed line) to the magnetic field. Bottom panel: Suprathermal tails decrease as a power law of the square velocity and are emphasized by comparison to the Maxwellian core (solid line)

Even if they don't contribute much to the number density, the enhanced population of suprathermal particles (especially the anisotropic part in the direction parallel to the magnetic field line) significantly modify the escape flux, the temperature and the heat flux, as it has been shown with models based on Kappa distributions or on a sum of two Maxwellians with different temperatures [2, 3]. Macroscopic parameters like density, average (flowing) velocity, pressure, temperatures in parallel and perpendicular

directions, heat flux, can be calculated as moments of the distribution function *f* by integrating in the velocity space. Velocity distribution functions (VDF) observed at different radial distances show the radial evolution of these parameters (density, bulk velocity and temperatures) [4]. Kinetic models allow to take into account non-thermal features of the distributions, e.g., kinetic anisotropies (beams, temperature anisotropy), suprathermal populations, such that they can provide a more detailed description of a (gas or) plasma than (magneto)hydrodynamic descriptions based on the equations relating the different moments.

These kinetic models are intended to resolve the evolution equation:

$$\frac{\partial f}{\partial t} + \vec{v} \cdot \frac{\partial f}{\partial \vec{r}} + \vec{a} \cdot \frac{\partial f}{\partial \vec{v}} = -\frac{\partial}{\partial \vec{v}} \cdot \left[\vec{A} f - \frac{1}{2} \frac{\partial}{\partial \vec{v}} \cdot \left(\vec{D} f \right) \right] + (WPI) \qquad (1)$$

where the acceleration ***a*** includes the gravity, the electric force and the Lorentz force due to the magnetic field in case of plasmas. The first term of right hand side (rhs) of eq. (1) represents the Fokker-Planck Coulomb collision term, the second term (WPI) represents the wave-particle interactions.

Models based on Vlasov equation where the collisional terms (in the rhs) are neglected, have already provided good results for the average moments above the exobase, where the interactions between the particles become negligible because the density of the particles becomes so low that the Knudsen number *Kn* is larger than 1 (*Kn=l/H* where *l* is the mean free path of the particles and *H* is the density scale height). In the solar wind, the exobase is located at low radial distances in the corona, between 1.1 and 5 Rs. Note also that the suprathermal particles are collisionless with a Kn well below that for the thermal (core) populations (already for $Kn > 0.01$), due to a strong velocity dependence of the Coulomb cross section [5].

SOLAR WIND MODELS

Vlasov Models

Solar wind models based on Vlasov equations have been developed enabling to understand the physical mechanisms implicated in the acceleration of the particles. These models provide satisfactory confirmations for the values of the average moments, and they are computationally economic because the moments can be calculated analytically. These arguments make them very suitable for solar wind predictions. Kappa distributions are assumed at the exobase for the electrons. Low values of the parameter kappa are associated to an enhanced population of suprathermal electrons leading to higher velocities at large radial distances [6].

To obtain precise boundary conditions is the main challenge, allowing us to make good predictions in three dimensions at larger distance in the heliosphere, but especially at the orbit of the Earth since solar wind variations can generate disturbances in the space environment of the Earth. To obtain these boundary conditions, we use as observational input photospheric magnetograms, i.e. the magnetic field at the photosphere as observed by GONG (Global Oscillation Network Group, see http://gong.nso.edu/). The initial magnetic field is then reconstructed using a potential field source surface (PFSS) scheme to provide the magnetic field (B_r, B_θ, B_ϕ) from the photosphere up to 2.5*R*s, corresponding to the source surface [7]. Above the source surface, the magnetic field is assumed to be purely radial. The magnetic field reconstruction is illustrated in Fig. 2 and allows to associate specific structures observed in the photosphere (like coronal holes and sunspots) to specific solar wind sources.

Conditions of densities, Kappa indexes (associated to velocity) and temperatures at the exobase level are then associated to the magnetic field characteristics on the basis of previous observations. All of these are used as boundary conditions at the exobase (chosen in our model to be at 2.5 Rs) to obtain an extended radial profile of the velocity distribution functions of the particles from the corona to the whole heliosphere. To obtain the best empirical relations providing the moments at the exobase, observations of OMNI at 1 AU were used as boundary conditions in steady state models [8]. An example of the velocity obtained in the ecliptic plane for September 2008 is illustrated in Fig. 3.

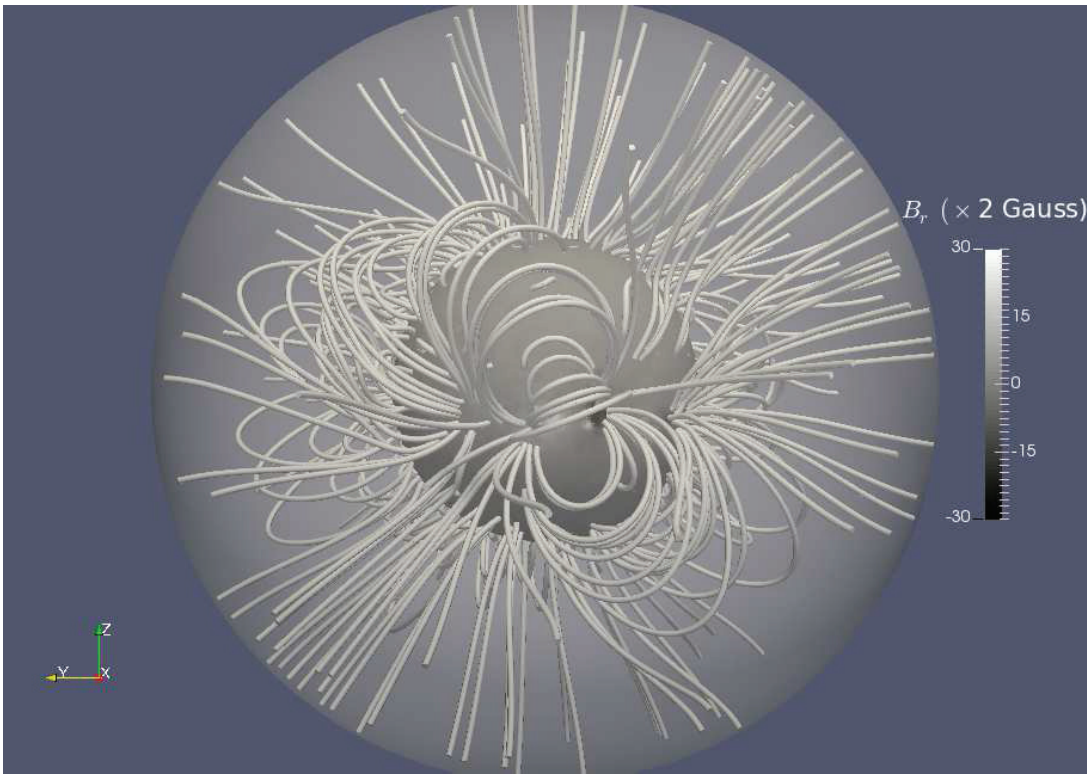

FIGURE 2. Global view of the solar magnetic field topology from the photosphere to the source surface at 2.5R_s observed for the synoptic map of CR2059 in July-August 2007

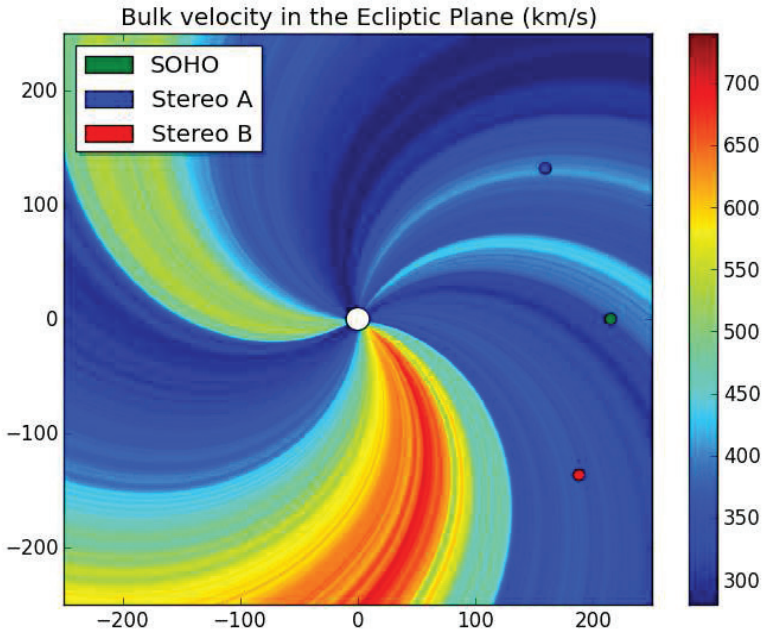

FIGURE 3. Solar wind velocity found for Carrington Rotation 2075 with the kinetic solar wind model. The positions of SOHO, Stereo A and B spacecraft are also illustrated

However, we are not limited to the ecliptic plane: the latitudinal dependence can also be obtained as illustrated in Fig. 4 and 5, respectively, for the electron number density and velocity obtained with the model at 1 AU for 10-8-2007 for instance. An undulating sheet with higher densities and lower velocities is clearly visible during this period of low solar activity. High speed solar wind associated to lower densities is obtained at high latitudes, as observed by ULYSSES [8]. We can also determine all the different moments at any distance larger than 2.5 R_s, since we have the velocity distribution functions in the whole heliosphere.

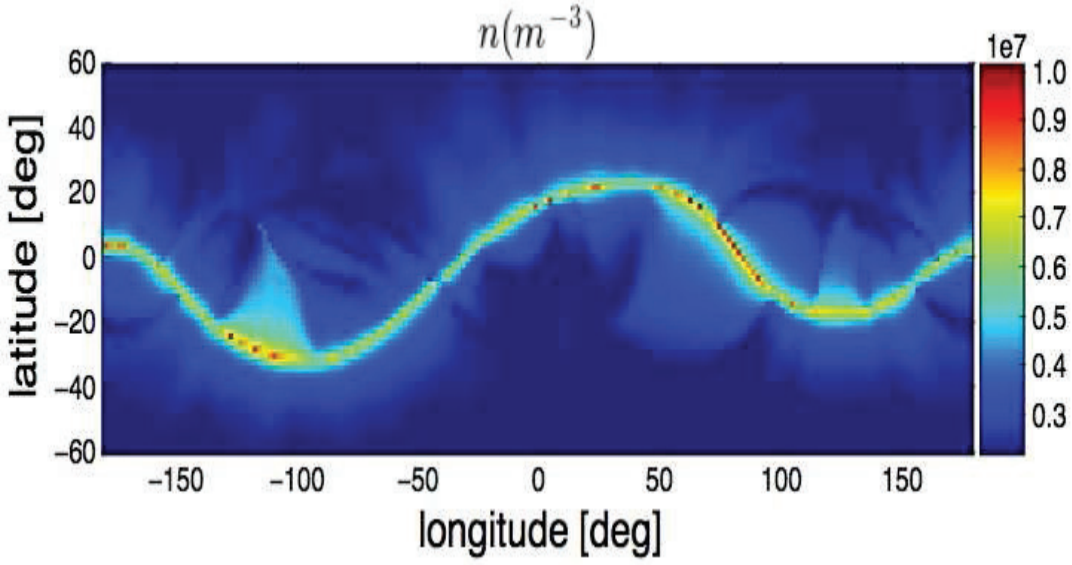

FIGURE 4. Solar density found at 1 AU on 10-8-2007 during solar minimum with the kinetic model of the solar wind as a function of heliographic latitude and longitude.

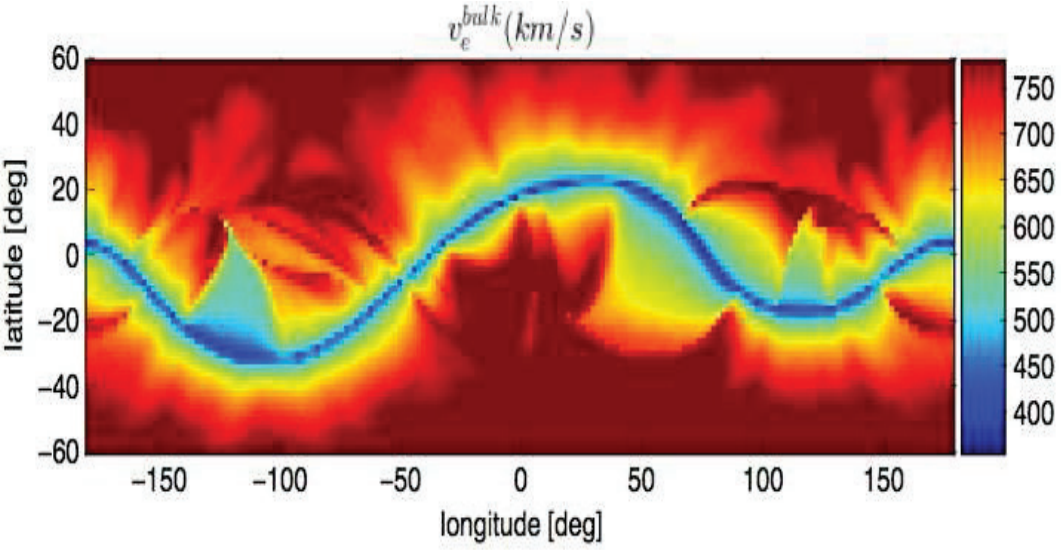

FIGURE 5. Solar wind velocity found at 1 AU on 10-8-2007 during solar minimum with the kinetic model of the solar wind as a function of heliographic latitude and longitude. The boundary conditions are based on photospheric magnetograms and are similar to those taken for MHD models. They lead to a low density at high latitudes and a undulating neutral sheet with higher densities

The results of our kinetic exospheric model has been compared with other semi-empirical models based on solution of the MHD equations. They provide the solution at a starting distance of about 21.5 R_s to avoid the inclusion of the sonic point in the computational domain. Our kinetic model is faster in computation time, can provide all the moments including heat flux and temperature anisotropy, and is not limited to electron and proton characteristics, since the other ions (even if present in low quantities) can also be included. Nevertheless, MHD takes better into account the actual magnetic field configuration at all radial distances [9]. The principle to link the magnetic field characteristics to obtain precise boundary conditions was inspired by the success of the WSA (Wang-Sheeley-Arge) [10, 11] solar wind speed quantifications.

Fokker-Planck Models

To better understand the generation of the suprathermal particles and other specific features observed in the VDF of the particles, it is necessary to consider not only the interactions between particles (Coulomb collision term) but especially the interactions between particles and fluctuations present in the corona and the solar wind. A specific numerical method of expansion of the solution in orthogonal polynomials has been used to solve the equation, based on the works of [12] and especially the development of speed polynomials. Using the same method, new polynomials that converge faster in case of suprathermal particles were also developed [13]. To study the collision-dominated to collisionless transition region, we use specific boundary conditions: in the collision-dominated region at very low altitudes in the corona, the upward part of the electron VDF is assumed to be Maxwellian, while exospheric conditions are assumed at the the top collisionless region. It was shown that the VDF of the electrons becomes more and more anisotropic with the the radial distance, in direct relation with the creation of the wind [14]. Nevertheless, to obtain the halo population visible also in the direction perpendicular to the magnetic field lines, an additional effect has to dominate at large velocities. Pierrard et al. (2011) showed that whistler wave turbulence can be a good candidate [15]. For the protons, the tail is more associated to the presence of kinetic Alfvén waves, and the second peak called the proton beam can be generated in case of spatially varying Alfvén waves [16, 17]. With the kinetic evolution equation, each term can be associated to each effect and studied separately.

PLASMASPHERE MODEL

Kinetic models of space plasmas are not limited to the solar wind. They can be used for the exosphere of the other stars and of the planets (note that similar exospheric models are also developed for neutral gas of planetary atmospheres). They were used for the exosphere of Mars [18], Saturn and Jupiter and their main moons [19], and in a very detailed way for the Earth. Along open magnetic field lines, polar wind allows light ions to escape [20], while along closed field lines, the ionized particles of the ionosphere are trapped in the magnetic field [21]. Both regions have also been modelled at BIRA-IASB using the kinetic approach. The 3DPS plasmasphere model is coupled with International Reference Ionosphere that is used to determine the boundary conditions at 700 km. An example of the electron density provided by the plasmasphere kinetic model is illustrated in Fig. 6 in the equatorial and meridian plane. The model, available for free run at any date on www.spaceweather.eu, provides also the temperature and is dynamic since the position of the plasmapause (the limit of the plasmasphere where sharp density gradients are observed) is highly variable with time and geomagnetic conditions (associated to the solar wind variations). The results provide good comparisons with satellite measurements [22, 23, 24].

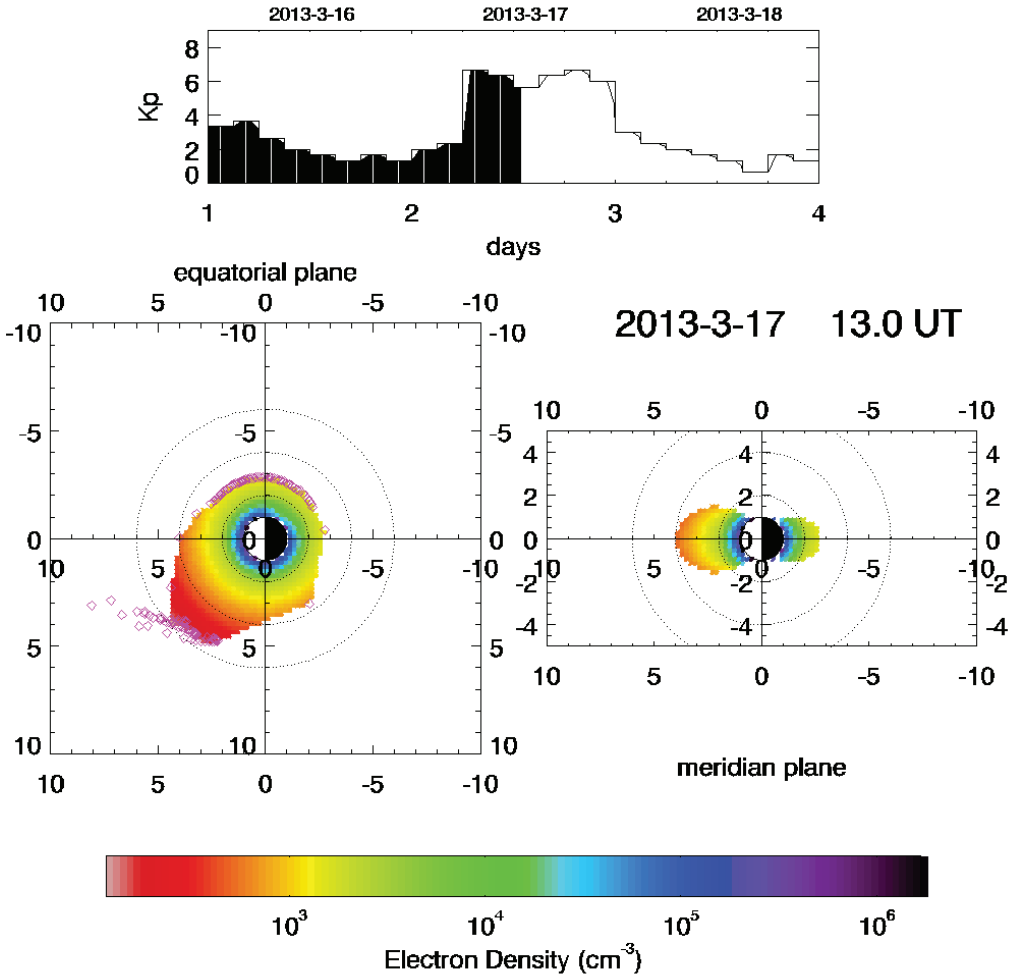

FIGURE 6. Electron density in the Earth's plasmasphere obtained with the kinetic model for the date of 17 March 2013 on 13:00 UT in the equatorial plane (left panel) and meridian plane (right panel). A plume appears during this geomagnetic storm in the afternoon MLT (Magnetic Local Time) sector due to the increase of geomagnetic activity illustrated by the planetary index Kp on the upper panel

RADIATION BELTS

Much more energetic particles (MeV, instead of eV for the plasmasphere) are also trapped in the magnetic field of the Earth. They are much more rarefied, but dangerous for spacecraft and astronauts, that is why reliable models are especially important to predict the impact of these particles, and quantify their effects. The plasmasphere and radiation belts partially overlap and interactions between the low energy and high energy particles have been deduced from observations [25]. To study the physical mechanisms that are active in the radiation belts, we simulate their trajectories by launching particles with different energies. Their motion can be decomposed in three superposed movements: gyration around the field lines, oscillation between two mirror points located in each hemisphere and azimuthal drift to East for electrons and West for protons [26].

An example of such simulations is illustrated in Fig. 7. When the magnetic field is disturbed during a geomagnetic storm generated by a solar wind event, the particle can be lost, as illustrated on the right panel, or accelerated to higher energies and the simulations allow to determine how their trajectories are modified.

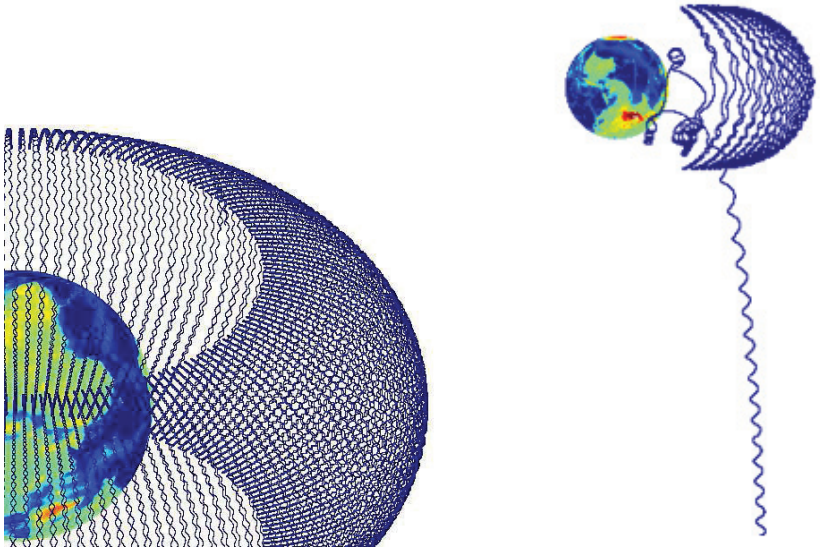

FIGURE 7. Simulation of the trajectory of a 1 MeV proton trapped in the magnetic field of the Earth. The motion can be decomposed in three superposed motions: gyration around the field line, oscillation between two mirror points in each hemisphere and azimuthal drift. When the magnetic field is disturbed during a geomagnetic storm, the particle can be lost (right panel)

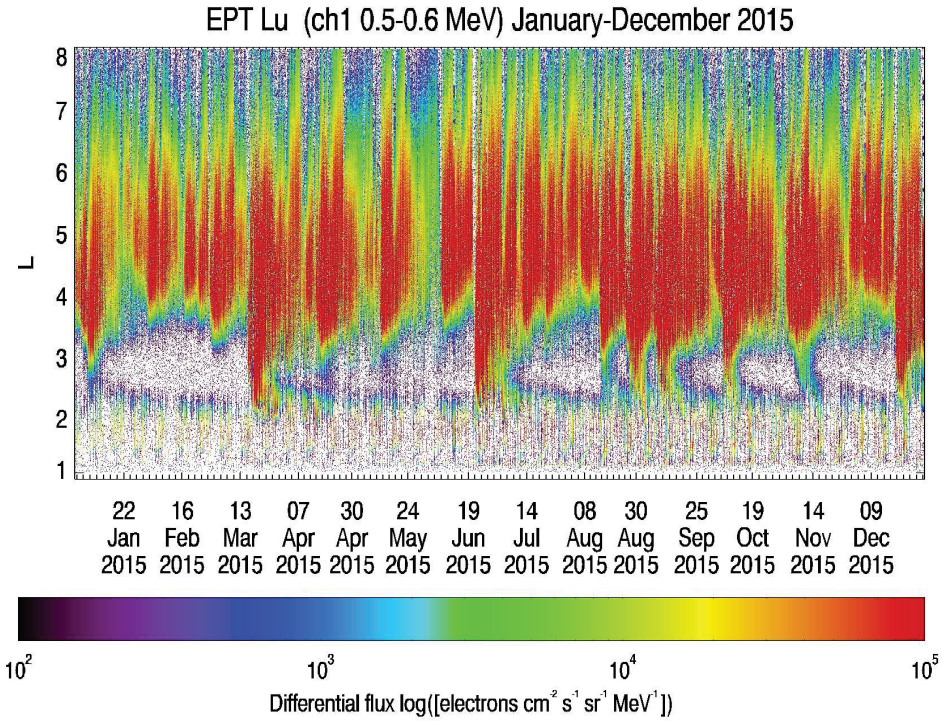

FIGURE 8. Electron fluxes measured by the EPT instrument in the energy range 500-600 keV during the year 2015 as a function of the McIlwain parameter L corresponding to the Earth's radial distance at the equator in Earth radii (Re). The flux is highly variable during this very active year, with injections at low distances during geomagnetic storms appearing in January, March, June, August, September, November and December

Empirical models based on satellite data remain nevertheless often used in these regions where the physical mechanisms implicated in the source, loss and radial transport of the particles are complex. Reliable non contaminated measurements of the particle fluxes are also difficult to obtain. That is why we contributed to the development of a new instrument called the Energetic Particle Telescope (EPT) [27]. Launched in May 2013 on the ESA satellite PROBA-V, the EPT instrument provides high resolution fluxes with excellent discrimination between the particles (electrons, protons and helium ions) [28]. During the year 2015, strong geomagnetic storms were observed [29], with injections of energetic electrons at lower radial distances, as illustrated in Fig. 8.

CONCLUSIONS

Kinetic processes prevail in space plasmas where the number density is so low that the Knudsen number is higher than 1. Even when the Knudsen number is lower than 1, the suprathermal particles are already collisionless, due to the strong dependence of the Coulomb collisions on the velocity of the particles. Kinetic models based on Fokker-Planck equation allow to study the effects of collisions, but also to include wave-particle interactions like whistler waves for electrons and kinetic Alfvén waves for the protons. These effects can explain the presence of halo and anisotropic features observed in the VDF of the particles measured in space plasmas. But kinetic models based on the simpler Vlasov equation remain interesting for predictions due to fast calculation. Such kinetic models have been developed for many different space plasmas (and also neutral gas), including the solar wind, different regions of the Earth's magnetosphere and for the exosphere of other planets. They can be adapted, following the same principles, to other space environments and atmospheres.

ACKNOWLEDGMENTS

This research work received support of the Scientific Federal Policy, in the framework of the program Interuniversity Attraction Pole for the project P7/08 CHARM and for the EPT project. The authors acknowledge financial support from the Alexander von Humboldt Foundation (ML) , BELSPO-PRODEX and FWO-Vlaanderen (VP, SM and ML).

REFFERENCES

1. V. Pierrard and M. Lazar, Sol. Phys. **287**, 153-174, doi: 10.1007/s11207-010-9640-2 (2010)
2. V. Pierrard, "Effects of suprathermal particles in space plasmas", in *Physics of the heliosphere: A 10 year retrospective,* AIP Conference Proceedings 1436, 61-66, doi: 10.1063:1.4723591 (2012).
3. N. Meyer-Vernet, *Basics of the Solar Wind* (Cambridge University Press, Cambridge, 2007).
4. V. Pierrard, M. Lazar , S. Poedts, S. Stverak, M. Maksimovic, P. M. Tranicek, ,Sol. Phys., **291**(7), 2165-2179, doi: 10.1007/s11207-016-0961-7 (2016).
5. J. D. Scudder and H. Karimabadi, Astrophys. J. **770**, 11 (2013).
6. V. Pierrard and J. Lemaire, J. Geophys. Res**. 101**, 7923-7934 (1996).
7. S. Moschou, "Solar Wind Modelling: MHD And Kinetic Treatments",Ph.D. thesis, Katholiek Universiteit Leuven, 2016.
8. V. Pierrard and M. Pieters, J. Geophys. Res, **119**, 9441-9455, doi: 10.1002/2014JA020678 (2014).
9. R. Keppens, Z. Meliani, A. J. van Marle, P. Delmont, A. Vlasis, and B. van der Holst, J. Comput. Phys. **231**, 718–744, doi: 10.1016/j.jcp.2011.01.020 (2012).
10. Y.-M. Wang and N. R. Sheeley Jr., *ApJ*, **355**, 726–732, doi: 10.1086/168805 (1990).
11. C. N. Arge and V. J. Pizzo, J. Geophys. Res. **105**, 10465–10480, doi: 10.1029/1999JA000262 (2000).
12. B. Shizgal and R. Blackmore, J. Comput. Phys **55**, 313 (1984).
13. A. P. Magnus and V. Pierrard, J. Comput. Applied Math. **219**, 431-440 (2007).
14. V. Pierrard, M. Maksimovic and J. Lemaire, J. Geophys. Res. **107**, A12, 29.305-29.312 (2001).
15. V. Pierrard, M. Lazar and R. Schlickeiser, Sol. Phys. **269**, 421-438, doi :10.1007/s11207-010-9700-7 (2011).
16. V. Pierrard and Y. Voitenko, Sol. Phys. **288**, 369-387, doi: 10.1007/s11207-013-0296-6 (2013).
17. Y. Voitenko and V. Pierrard, Sol. Phys. **290**, 1231-1241 (2015).
18. V. Pierrard, Planet. Space Sci. **51**, 319-327 (2003).
19. V. Pierrard, Planet. Sp. Sci. **57**, 1260-1267, doi : 10.1016/j.pss.2009.04.011 (2009).

20. S. W. Y. Tam, T. Chang, V. Pierrard, J. Atmosph. Sol. Terr. Phys. **69**, 1984- 2027, doi: 10.1016/j.jastp.2007.08.006 (2007).
21. V. Pierrard and M. Voiculescu, Geophys. Res. Lett. **38**, L12104, doi:10.1029/2011GL047767 (2011).
22. V. Pierrard and J. Cabrera, Space Science Reviews **122**, 119-126, doi: 10.1007/s11214-005-5670-8 (2006).
23. G. Verbanac, V. Pierrard, M. Bandic, F. Darrouzet, J.-L. Rauch and P. Décréau,, Annal. Geophys. **33**, 1271-1283, doi:10.5194/angeo-33-1271-2015 (2015).
24. M. Bandic, G. Verbanac, M. Moldwin, V. Pierrard, and G. Piredda, J. Geophys. Res. **121**, 4397-4408,doi: 10.1002/2015JA022278 (2016).
25. F. Darrouzet et al., J. Geophys. Res.: Space Phys. **118**, 4176-4188, doi: 10.1002/jgra.50239 (2013).
26. J. F. Lemaire, S.G. Batteux, and I.N. Slypen, Journal of Atmospheric and Solar-Terrestrial Physics **67**, 719-727 (2005).
27. M. Cyamukungu et al., IEEE Trans. Nucl. **61**, 3667-3681, doi: 10.1109/TNS.2014.2361955 (2014).
28. V. Pierrard et al., Space Science Rev. **184**, 87-106, doi: 10.1007/s11214-014-0097-8 (2014).
29. V. Pierrard and G. Lopez Rosson, Ann. Geophys. **34**, 75-84, doi:10.5194/angeo-34-75-2016 (2016).